Hindawi Publishing Corporation
Journal of Nanomaterials
Volume 2015, Article ID 489029, 6 pages
http://dx.doi.org/10.1155/2015/489029

Research Article

Microwave-Solvothermal Synthesis of Nanostructured BiOBr with Excellent Visible-Light Photocatalytic Properties

Shuisheng Wu, Qian Dong, Jun Wang, Qingming Jia, Yanlin Sun, Shaoyun Shan, and Yaming Wang

Faculty of Chemical Engineering, Kunming University of Science and Technology, Kunming 650500, China

Correspondence should be addressed to Yaming Wang; wangymkmust@126.com

Received 17 September 2014; Revised 27 November 2014; Accepted 8 December 2014

Academic Editor: Shaobin Wang

Novel BiOBr hierarchical microspheres have been successfully prepared via a facile microwave-assisted solvothermal route and used for visible-light photocatalytic degradation of RhB. The phase and morphology of the products were characterized by powder X-ray diffraction (XRD), thermogravimetric analysis (TG), scanning electron microscopy (SEM), BET, and UV-vis diffuse reflectance spectra. The SEM observations displayed that BiOBr flower-like nanostructure assembled from nanosheets. The BiOBr flower-like nanostructure, with a narrow band gap (2.63 eV), shows excellent photocatalytic activity in the degradation of RhB dye under visible-light, much higher than those of BiOBr nanosheet and P25 photocatalysts.

1. Introduction

BiOBr as one of the ternary compounds has aroused tremendous interest amidst scientific communities, since it can be used as photocatalysts [1–3] and as pigments in the cosmetic industry [4]. In view of the fact that the unique properties of nanomaterials are structure dependent [5–7], scientists have paid much attention to the controllable synthesis of BiOBr with nanosized particles such as hydrolysis process [8, 9], reverse microemulsion synthesis [10], and solvothermal process [11] and of hierarchical microspheres morphology [12–18]. By means of hydrothermal and/or solvothermal treatment at 140–180°C for 10–24 h and with or without template, BiOBr nanobelts [19], nanoflakes and nanoplates [2, 9], and microspheres and nanoflowers [12–15] have been successfully prepared.

In recent years, microwave-hydrothermal reaction has been used as an effective method for the synthesis of nanoparticles of various oxides [20, 21]. Compared with conventional methods, microwave-hydrothermal synthesis has many distinct advantages: (1) shorter reaction time, (2) more uniform product dimensions and composition, and (3) easiness to tune compositions of the products [22, 23]. Herein, we report the successful synthesis of BiOBr hierarchical microspheres constructed by nanosheets through a facile and rapid microwave-assisted solvothermal route. Furthermore, the visible-light photocatalytic properties of BiOBr samples were studied.

2. Experiment Section

2.1. Synthesis. All the chemicals were of analytic purity and used without further purification. In a typical process, 2 mmol $Bi(NO_3)_3{\cdot}5H_2O$ and 2 mmol cetyltrimethylammonium bromide (CTAB) were dissolved into 40.0 mL ethylene glycol solution while stirring for 10 min at room temperature, respectively. Then, CTAB solution was added dropwise to $Bi(NO_3)_3{\cdot}5H_2O$ solution in turn. After being vigorously stirred for 30 min at room temperature, the final clear buffy solution was transferred to a Teflon vessel of the MDS-6 (Microwave Digestion/Extraction System, Shanghai Sineo Microwave Chemical Technology Co., Ltd.) with 80% volume filled. The microwave treatment was maintained at 160°C for various reaction time (10, 30, 60, and 120 min, which were denoted as BiOBr-1, BiOBr-2, BiOBr-3, and BiOBr-4, resp.) under autogenous pressure and then naturally cooled to room temperature. The as-prepared yellow powders were repeatedly washed with the distilled water and ethanol three times, filtered, and dried in an oven at 60°C.

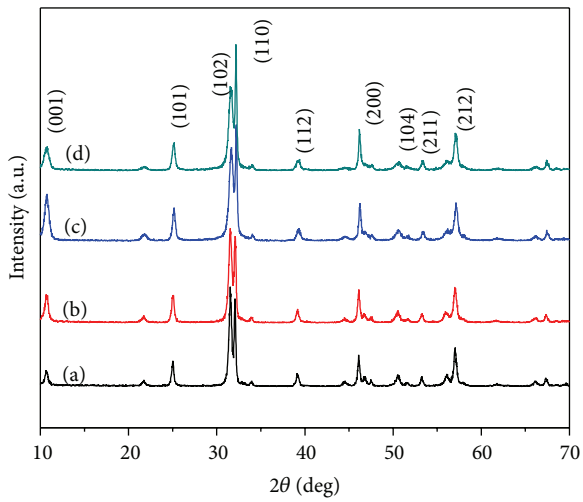

Figure 1: XRD pattern of BiOBr sample: (a) BiOBr-1, (b) BiOBr-2, (c) BiOBr-3, and (d) BiOBr-4.

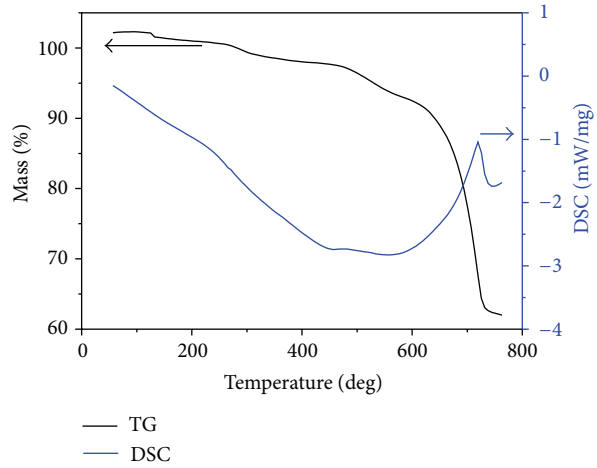

Figure 2: TG-DSC curves of BiOBr-4.

2.2. Characterization. The phase of as-synthesized samples was studied by X-ray diffraction (XRD) with a Bruker D8 Advance diffractometer (using Cu K_α radiation (λ = 1.54056 Å) and operating at 40 kV and 40 mA). The morphology of as-prepared samples was examined by scanning electron microscopy (SEM, HITACHI S-4800) and high resolution transmission electron microscopy (HRTEM, JEM-2100). N_2 adsorption-desorption isotherms were measured on a Quantachrome NOVA 4000e at 77 K. The Brunauer-Emmett-Teller (BET) method was used to calculate the specific surface area. The thermal stability was investigated by a thermogravimetric analyzer (TG 209 F1, NETZSCH). The optical property was analyzed by UV-vis diffuse reflectance spectra (DRS, UV-2400PC, SHIMADZU) equipped with ISR-240A type integrating sphere.

2.3. Photocatalytic Test. The photocatalytic activities of the as-synthesized BiOBr flowers were evaluated in terms of the degradation of RhB in an aqueous solution. A 250 W high-pressure mercury lamp (dominant wavelength: 365 nm) used as light source was positioned inside a cylindrical vessel and surrounded by circulating water jacket for cooling. To make sure that the photocatalytic reaction was really driven by visible-light, all the UV lights with the wavelength less than 420 nm were removed by a glass filter (UVCUT420). 50 mg of sample was suspended in 50 mL of $2 * 10^{-5}$ mol/L RhB. The solution was continuously stirred for about 30 min at room temperature to ensure the establishment of an adsorption-desorption equilibrium among the photocatalyst, RhB, and water before irradiation with UV light from the high-pressure mercury lamp. At given time intervals, the concentration of RhB left in the solution was determined by the UV-vis spectroscopy (Shanghai Meipuda Instrument Co., Ltd., UV-1600) at its characteristic wavelength of 553 nm.

3. Results and Discussion

The phase and crystallographic structure of the as-obtained samples were examined by XRD. Figure 1 presents the XRD pattern of the as-synthesized BiOBr sample. The XRD pattern can clearly demonstrate that the product is well crystalline and all the diffraction peaks can be indexed unambiguously to pure tetragonal BiOBr with lattice constants $a = b =$ 3.926 Å and $c =$ 5.208 Å, well consistent with the standard PDF database (JCPDS 09-0393) [24]. The crystallite sizes of BiOBr-1, BiOBr-2, BiOBr-3, and BiOBr-4 calculated by the Scherrer equation ($D = K\lambda/\beta * \cos\theta$) based on the principal (110) diffraction peak are 11, 12.5, 18.0, and 28.0 nm, respectively. It means that increasing the solvothermal time can enhance the crystallization of BiOBr catalyst. No other peaks corresponding to impurities are detected, showing that the final products purely consist of BiOBr.

Figure 2 shows the TG and DSC curves of the BiOBr-4 photocatalyst. The TG curve shows that no significant mass loss was recorded from room temperature to 600°C. It demonstrates that the BiOBr sample is steady below 600°C, so the prepared samples are of good stability and purity under the reaction temperature (room temperature) [15]. The litter mass loss may be caused by the evaporated water molecules. The mass of BiOBr sharply decreased from 600°C with an exothermic peak on the DSC curve, indicating the decomposition of BiOBr. And remarkable exothermic phenomenon is observed at 600–800°C, which may be caused by substance change.

The microstructure and morphology of the product were investigated by SEM. The SEM images of the resulting products are presented in Figure 3. At the initial time of 10 min, small nanosheets in irregular shape were formed with the in-plane size of about 150–300 nm and thickness of about 20–30 nm. Then, the nanosheets exhibited the gradual agglomeration and oriented attachment at 30 min. As the solvothermal time prolonged to 60 min, the integrate flower-like microspheres were formed with larger and thinner nanosheets (about 15 nm thickness). Further increasing the solvothermal time to 120 min could achieve the larger microspheres, in which the diameter was about 1.3–1.5 μm and the nanosheet thickness was about 20 nm. Based on the above SEM morphology, the plausible mechanism of BiOBr crystal

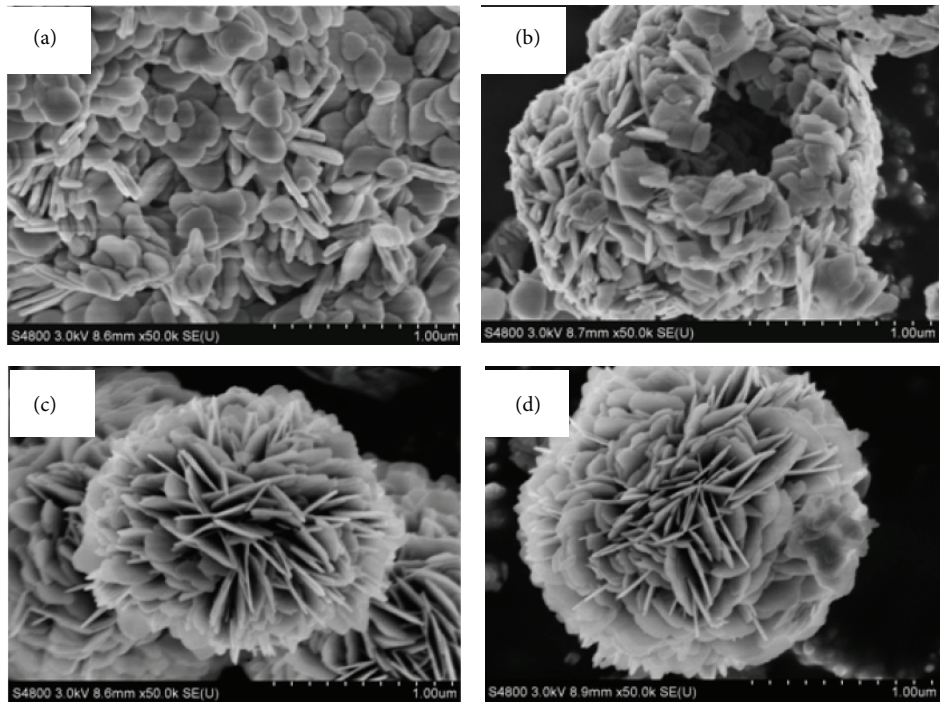

Figure 3: SEM images of BiOBr sample: (a) BiOBr-1, (b) BiOBr-2, (c) BiOBr-3, and (d) BiOBr-4.

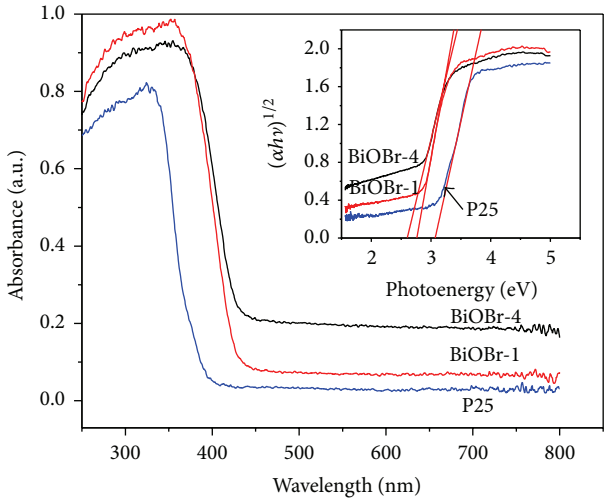

Figure 4: UV-vis diffuse reflectance spectra of the BiOBr sample.

growth could be proposed. Before the solvothermal reaction, the coordination occurs between ethylene glycol and Bi^{3+} and generates stable five-membered-ring coordination cations ($Bi(OCH_2CH_2OH)^{2+}$), which was stable as a dense and linearly aligned structure. CTAB surfactant which acted as both template and Br source was self-assembled to form the lamellar structure [25]. The combination of Br^- in CTAB lamellas with $Bi(OCH_2CH_2OH)^{2+}$ induced the formation of BiOBr nanosheets during the solvothermal process. With the reaction time prolonged, the BiOBr nanosheets were agglomerating via the oriented attachment mechanism. In the following growth stage, nanosheets grow into three-dimensional (3D) flower-like hierarchical architectures built from oriented nanorods via self-assembly, driven by the minimization of the total energy of the system [26, 27]. However, the exact formation mechanism for the eventual microstructure and morphology by interaction between the nanoparticles is still unclear at the present time.

The optical properties of the as-prepared BiOBr-4 and BiOBr-1 were characterized by UV-vis diffuse reflectance spectroscopy and the result was shown in Figure 4. For a crystalline semiconductor, the optical absorption near band edge follows the formula $(\alpha h\nu)^n = A(h\nu - E_g)$ where α, h, ν, E_g, and A are the absorption coefficient, Plank constant, light frequency, band gap, and a constant, respectively [2, 28]. BiOBr is an indirect-gap semiconductor; n equals 1/2. The inset of Figure 4 shows the $(\alpha h\nu)^{1/2}$ versus $(h\nu)$ curve of the sample. By extrapolating the straight portion of $(\alpha h\nu)^{1/2}$-to-$(h\nu)$ plot to the $\alpha = 0$ point, the band gap of BiOBr-4 and BiOBr-1 was 2.63 and 2.75 eV, which was a key factor in determining its visible-light photocatalytic activity and is close to the value reported in other literatures [15, 24]. Furthermore, BiOBr-4 showed higher visible-light absorption than BiOBr-1, implying that more light reflection could be achieved within flower-like microspheres assembled with nanosheets.

N_2 adsorption-desorption technique was carried out to investigate the surface area of the BiOBr-10 and BiOBr-120, and the results are given in Figure 5. Type III isotherms were obtained for BiOBr-1 and BiOBr-4. The Brunauer-Emmett-Teller (BET) surface areas of the BiOBr-4 flower nanostructure (28.3 cm^2/g) are larger than that of BiOBr-4 nanosheets (10.4 cm^2/g). The large surface area can be due to

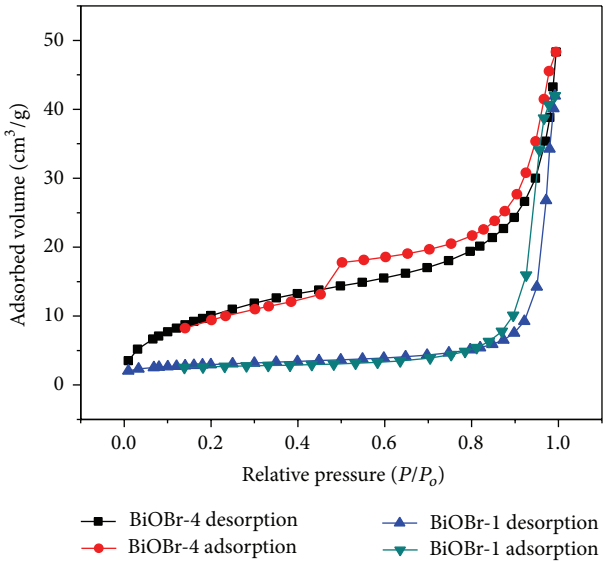

FIGURE 5: N_2 adsorption-desorption of the BiOBr sample.

its flower-like structure, which is beneficial for the diffusion of reactants and intermediates during reaction.

Rhodamine B (RhB), a widely used dye, was selected as the model pollutant to evaluate the photocatalytic activity. Its characteristic absorption at about 553 nm has been used to monitor the photocatalytic degradation process [29]. The photodegradation of RhB under visible-light irradiation ($\lambda >$ 420 nm) was used as a probe to evaluate the performances of different photocatalysts. Figure 6(a) shows the photocatalytic degradation of RhB on BiOBr sample, presenting the concentration changes of RhB during the degradation process. The degradation of RhB in the absence of photocatalyst is less than 5% at 90 min, which could be neglected. About 93%, close to 100% of RhB, was degraded within 40 min by the sample BiOBr-4, suggesting that the as-synthesized BiOBr hierarchical nanostructure possesses intrinsic photocatalytic activity. As for samples BiOBr-1 and P25, the degradation rate was 75% and 33% of RhB within 90 min. It is evident that the sample BiOBr-4 exhibited higher photocatalytic activity than that of samples BiOBr-1 and P25. It could be attributed to the fact that the hierarchical flower-like morphology assembled with nanosheets in BiOBr-4 with larger BET surface than nanosheet structure of BiOBr-4. Additionally, the hierarchical nanostructures could provide more efficient transportation of reactants in order to improve the photocatalytic activity.

The photocatalysis kinetics of the RhB by BiOBr was obtained by fitting the experimental data to pseudo-first-order model, and the pseudo-first-order model equation can be expressed by [30],

$$\ln\left(\frac{C}{C_0}\right) = -kt. \quad (1)$$

The C_0 and C are the concentrations of organic dye in solution at times 0 and t, respectively, and k is the pseudo-first-order rate constant. Figure 6(b) is the photocatalytic

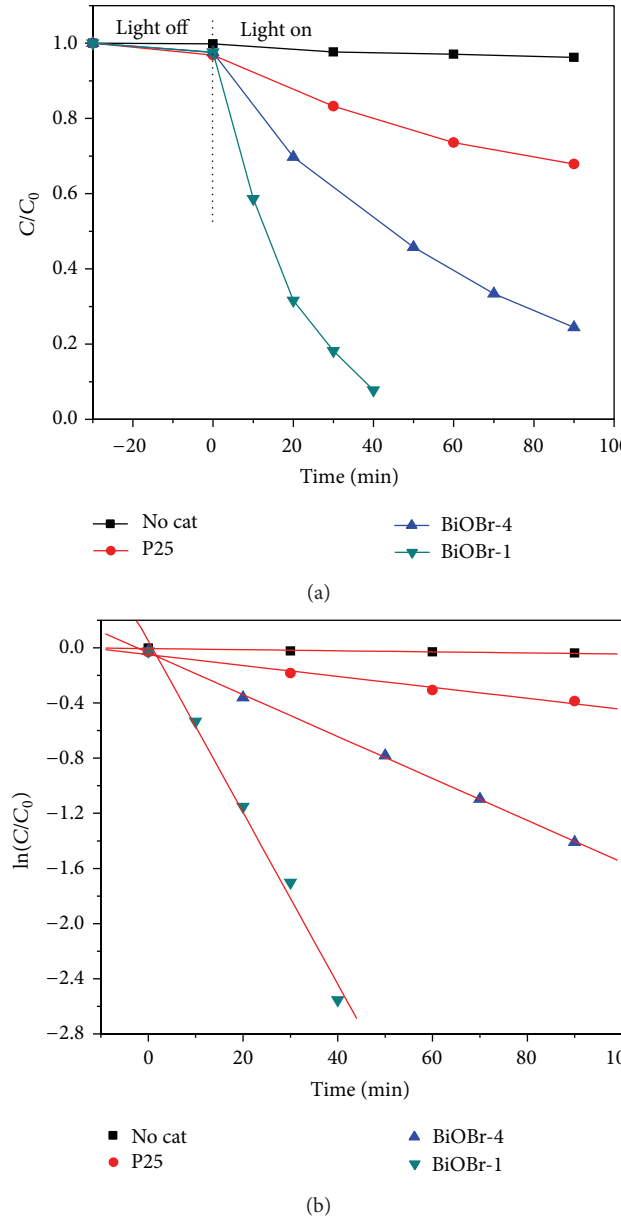

FIGURE 6: (a) Photodegradation efficiencies of RhB as a function of irradiation time; (b) photocatalysis kinetics of the RhB degradation. C_0 and C referred to the initial RhB concentration and the RhB concentration determined at different reaction time, respectively.

reaction kinetics of RhB degradation in solution on the basis of the data plotted in Figure 6(a). As can be seen, a rather good correlation to the pseudo-first-order reaction kinetics is found. When BiOBr-4, BiOBr-1, and P25 were used as photocatalyst, the pseudo-first-order rate constants are 0.0623 (R = 0.99), 0.0152 (R = 0.99), and 0.0040 (R = 0.99) min^{-1}, respectively, where the degradation rate constant of BiOBr-4 is four times higher than BiOBr-1 and fifteen times higher than P25. Several reasons may account for the high photocatalytic activity of the sample. First, the BET surface areas of the BiOBr-4 flower nanostructure (28.3 cm^2/g) are larger than that of BiOBr-4 nanosheets (10.4 cm^2/g), which

lead to more unsaturated surface coordination sites exposed to the pollution molecules in solution. This allows more efficient transport for the reactant molecules to the active sites, hence enhancing the efficiency of photocatalysis. Second, the high photocatalytic activity is not only related to the specific surface area but also associated with hierarchical structure. The rate constant of BiOBr-4 BiOBr-1 is $0.0022\,\mathrm{min}^{-1}\cdot\mathrm{m}^{-2}$ after being normalized by the surface area, which is 1.5 times higher than that of BiOBr-1 ($0.00146\,\mathrm{min}^{-1}\cdot\mathrm{m}^{-2}$); the reason may be attributed to the fact that the hierarchical microspheres composed of high surface-to-volume ratios of nanosheets are in favor of the transfer of electrons and holes and facilitate the degradation of pollution molecules.

The lifetime of photocatalyst is important for practical applications. The photodegradation of RhB over BiOBr-4 has been repeated 5 times under the same reaction conditions, by repeating the centrifugation of the BiOBr sample after completing the photocatalysis reaction and redispersing into 50 mL RhB solution in each run. In the lifetime test, photodegradation of RhB was 92.3%, 92.0%, 91.6%, 91.8%, and 91.5%, which indicates that BiOBr-4 exhibits nearly similar photocatalysis performance. It proves that BiOBr is stable and suitable for photocatalyst.

4. Conclusions

In summary, a novel BiOBr hierarchical microsphere has been successfully prepared via a facile microwave-assisted solvothermal route. The obtained BiOBr nanostructure is indirect transition semiconductors with intrinsic optical band gaps of approximately 2.63–2.75 eV depending on the synthesis conditions. These BiOBr flower-like nanostructures are more active for photodegradation of RhB dye under visible-light irradiation. Our work provides a facile, rapid, low-cost pathway to novel BiOBr hierarchical nanostructures.

Conflict of Interests

The authors declare that there is no conflict of interests regarding the publication of this paper.

Acknowledgments

This work was supported by the National Natural Science Foundation (21401088), Kunming University of Science and Technology doctoral scientific research fund (KKSY201205025), and Testing and Analyzing Foundation of KMUST.

References

[1] W. D. Wang, F. Q. Huang, X. P. Lin, and J. H. Yang, "Visible-light-responsive photocatalysts *x*BiOBr-(1-*x*)BiOI," *Catalysis Communications*, vol. 9, no. 1, pp. 8–12, 2008.

[2] X. Zhang, Z. H. Ai, F. L. Jia, and L. Z. Zhang, "Generalized one-pot synthesis, characterization, and photocatalytic activity of hierarchical BiOX (X = Cl, Br, I) nanoplate microspheres," *Journal of Physical Chemistry C*, vol. 112, no. 3, pp. 747–753, 2008.

[3] J. Zhang, F. J. Shi, J. Lin et al., "Self-assembled 3-D architectures of BiOBr as a visible light-driven photocatalyst," *Chemistry of Materials*, vol. 20, no. 9, pp. 2937–2941, 2008.

[4] F. J. Maile, G. Pfaff, and P. Reynders, "Effect pigments—past, present and future," *Progress in Organic Coatings*, vol. 54, no. 3, pp. 150–163, 2005.

[5] Z. L. Wang and J. H. Song, "Piezoelectric nanogenerators based on zinc oxide nanowire arrays," *Science*, vol. 312, no. 5771, pp. 242–246, 2006.

[6] H. L. Xu and W. Z. Wang, "Template synthesis of multishelled Cu_2O hollow spheres with a single-crystalline shell wall," *Angewandte Chemie—International Edition*, vol. 46, no. 9, pp. 1489–1492, 2007.

[7] L. Zhou, W. Wang, H. Xu, S. Sun, and M. Shang, "Bi_2O_3 hierarchical nanostructures: controllable synthesis, growth mechanism, and their application in photocatalysis," *Chemistry A: European Journal*, vol. 15, no. 7, pp. 1776–1782, 2009.

[8] W. Wang, F. Huang, X. Lin, and J. Yang, "Visible-light-responsive photocatalysts *x*BiOBr-(1-*x*)BiOI," *Catalysis Communications*, vol. 9, no. 1, pp. 8–12, 2008.

[9] Z. Jiang, F. Yang, G. Yang et al., "The hydrothermal synthesis of BiOBr flakes for visible-light-responsive photocatalytic degradation of methyl orange," *Journal of Photochemistry and Photobiology A: Chemistry*, vol. 212, no. 1, pp. 8–13, 2010.

[10] J. Henle, P. Simon, A. Frenzel, S. Scholz, and S. Kaskel, "Nanosized BiOX (X = Cl, Br, I) particles synthesized in reverse microemulsions," *Chemistry of Materials*, vol. 19, no. 3, pp. 366–373, 2007.

[11] Z. H. Ai, W. k. Ho, S. C. Lee, and L. Z. Zhang, "Efficient photocatalytic removal of NO in indoor air with hierarchical bismuth oxybromide nanoplate microspheres under visible light," *Environmental Science and Technology*, vol. 43, no. 11, pp. 4143–4150, 2009.

[12] Y. Huo, J. Zhang, M. Miao, and Y. Jin, "Solvothermal synthesis of flower-like BiOBr microspheres with highly visible-light photocatalytic performances," *Applied Catalysis B: Environmental*, vol. 111-112, pp. 334–341, 2012.

[13] J. Xu, W. Meng, Y. Zhang, L. Li, and C. Guo, "Photocatalytic degradation of tetrabromobisphenol A by mesoporous BiOBr: efficacy, products and pathway," *Applied Catalysis B: Environmental*, vol. 107, no. 3-4, pp. 355–362, 2011.

[14] L. Zhang, X.-F. Cao, X.-T. Chen, and Z.-L. Xue, "BiOBr hierarchical microspheres: microwave-assisted solvothermal synthesis, strong adsorption and excellent photocatalytic properties," *Journal of Colloid and Interface Science*, vol. 354, no. 2, pp. 630–636, 2011.

[15] Y. C. Feng, L. Li, J. W. Li, J. F. Wang, and L. Liu, "Synthesis of mesoporous BiOBr 3D microspheres and their photodecomposition for toluene," *Journal of Hazardous Materials*, vol. 192, no. 2, pp. 538–544, 2011.

[16] G. Li, F. Qin, H. Yang, Z. Lu, H. Sun, and R. Chen, "Facile microwave synthesis of 3D flowerlike BiOBr nanostructures and their excellent Cr VI removal capacity," *European Journal of Inorganic Chemistry*, vol. 2012, no. 15, pp. 2508–2513, 2012.

[17] D. Q. Zhang, M. C. Wen, B. Jiang, G. S. Li, and J. C. Yu, "Ionothermal synthesis of hierarchical BiOBr microspheres for water treatment," *Journal of Hazardous Materials*, vol. 211-212, pp. 104–111, 2012.

[18] P. P. Xiao, L. L. Zhu, Y. C. Zhu, and Y. T. Qian, "Room-temperature synthesis of BiOBr sub-microflowers and their photocatalytic properties," *Journal of Nanoscience and Nanotechnology*, vol. 12, no. 3, pp. 2008–2013, 2012.

[19] C. F. Guo, J. Zhang, Y. Tian, and Q. Liu, "A general strategy to superstructured networks and nested self-similar networks of bismuth compounds," *ACS Nano*, vol. 6, no. 10, pp. 8746–8752, 2012.

[20] S. F. Liu, I. R. Abothu, and S. Komarneni, "Barium titanate ceramics prepared from conventional and microwave hydrothermal powders," *Materials Letters*, vol. 38, no. 5, pp. 344–350, 1999.

[21] A. Bonamartini Corradi, F. Bondioli, A. M. Ferrari, and T. Manfredini, "Synthesis and characterization of nanosized ceria powders by microwave-hydrothermal method," *Materials Research Bulletin*, vol. 41, no. 1, pp. 38–44, 2006.

[22] G. A. Tompsett, W. C. Conner, and K. S. Yngvesson, "Microwave synthesis of nanoporous materials," *ChemPhysChem*, vol. 7, no. 2, pp. 296–319, 2006.

[23] I. Bilecka, I. Djerdj, and M. Niederberger, "One-minute synthesis of crystalline binary and ternary metal oxide nanoparticles," *Chemical Communications*, no. 7, pp. 886–888, 2008.

[24] M. Shang, W. Z. Wang, and L. Zhang, "Preparation of BiOBr lamellar structure with high photocatalytic activity by CTAB as Br source and template," *Journal of Hazardous Materials*, vol. 167, no. 1–3, pp. 803–809, 2009.

[25] A. Lak, M. Mazloumi, M. Mohajerani et al., "Self-assembly of dandelion-like hydroxyapatite nanostructures via hydrothermal method," *Journal of the American Ceramic Society*, vol. 91, no. 10, pp. 3292–3297, 2008.

[26] L. Xu, J. Shen, C. Lu, Y. Chen, and W. Hou, "Self-assembled three-dimensional architectures of $Y_2(WO4)_3$:Eu: controlled synthesis, growth mechanism, and shape-dependent luminescence properties," *Crystal Growth and Design*, vol. 9, no. 7, pp. 3129–3136, 2009.

[27] L. Chen, S.-F. Yin, R. Huang, Y. Zhou, S.-L. Luo, and C.-T. Au, "Facile synthesis of BiOCl nano-flowers of narrow band gap and their visible-light-induced photocatalytic property," *Catalysis Communications*, vol. 23, pp. 54–57, 2012.

[28] S. Wu, H. Cao, S. Yin, X. Liu, and X. Zhang, "Amino acid-assisted hydrothermal synthesis and photocatalysis of SnO_2 nanocrystals," *The Journal of Physical Chemistry C*, vol. 113, no. 41, pp. 17893–17898, 2009.

[29] J.-M. Herrmann, H. Tahiri, Y. Ait-Ichou, G. Lassaletta, A. R. González-Elipe, and A. Fernandez, "Characterization and photocatalytic activity in aqueous medium of TiO_2 and Ag-TiO_2 coatings on quartz," *Applied Catalysis B: Environmental*, vol. 13, no. 3-4, pp. 219–228, 1997.

[30] R. G. Chen, J. H. Bi, L. Wu, Z. H. Li, and X. Z. Fu, "Orthorhombic Bi_2GeO_5 nanobelts: synthesis, characterization, and photocatalytic properties," *Crystal Growth and Design*, vol. 9, no. 4, pp. 1775–1779, 2009.